JOURNAL OF MATERIALS SCIENCE 31 (1996) 5985–5991

Acoustic emission and precision force–displacement observations of pointed and spherical indentation of silicon and TiN film on silicon

M. SHIWA
Tsurumi Research and Development Center, Japan Power Engineering and Inspection Corporation, 14-1 Benten-cho, Tsurumi-ku Yokohama, 251, Japan

E. WEPPELMANN, D. MUNZ
Instituts für Zuverlassigkeit und Schadenskunde im Maschinenbau, University of Karlsruhe, D-7500 Karlsruhe 1, Germany

M. V. SWAIN
National Measurement Laboratory, CSIRO Division of Applied Physics, Lindfield, NSW 2070, Australia

T. KISHI
Research Center for Advanced Science and Technology, The University of Tokyo, 13-1 Komaba Meguro-ku Tokyo, 153, Japan

Simultaneous measurements have been recorded of the force, displacement and acoustic emission (AE) during the loading and unloading of a spherical indentor on to a silicon and a physical–vapour deposited 2.7 μm thick TiN film on silicon. The AE signals were able to detect the formation of small cracks, such as Hertzian cracks, lateral cracks in silicon and to detect the onset of film cracking during loading and film delamination during unloading in TiN film. The measure data were also compared with SEM cross-section observations of the indented region. Excellent correlation between AE, force–displacement and SEM observation was found.

1. Introduction

Thin films deposited on cheaper substrates are now widely used for imparting optimum properties. However, as with all materials systems, the mechanical properties and the assessment of the reliability of such films are essential for engineering applications. To date, the most widely used means for such measurements are indentation and scratch testing; however, the physical interpretation of the data from such is often difficult.

Observation of indentation using a micro-spherical indentor of TiN films on a silicon substrate by Weppelmann *et al.* [1] revealed that two major cracking types were observed, such as circumferential cracks, which coincided with a small discontinuity on the loading curve, and readily apparent delamination cracks surrounding the residual impression.

The present study is an extension of a previous investigation by Weppelmann *et al.* [1] of the delamination of TiN films on a silicon substrate about spherical indentations. An expression for the interfacial fracture energy was developed during the course of that study based upon post-indentation estimation of the delamination crack size. It was also noted that most of the observed non-linear response during indentation was a consequence of the permanent deformation of the underlying silicon substrate. The nature of the response of the silicon during spherical indentation was also addressed by Weppelmann *et al.* [2] who were able to show that the force–displacement behaviour was controlled by the various phase transformations beneath the contact site.

A pervious study by Weihs *et al.* [3] investigated the use of acoustic emission during precision force–displacement indentation with a Berkovich indentor of various materials. They were able to detect the onset of deformation and cracking beneath the indentor. These authors were unable to detect, with acoustic emission (AE), the onset of phase transformation in silicon beneath, or radial crack in glass for, low-load Berkovich impressions.

The focus of the present study was on TiN films which are very widely utilized for coatings on metal working tools and have been shown to impart significant lifetime improvements. The hardness of such films is often considered as one of the key parameters

0022–2461

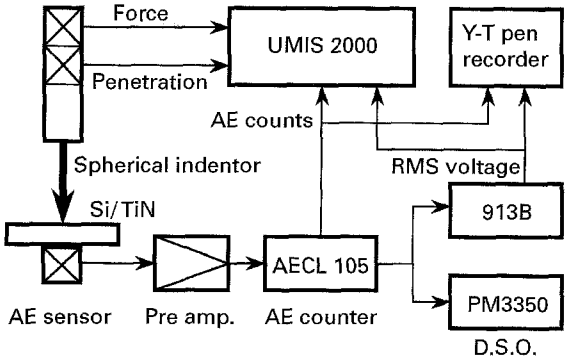

Figure 1 Block diagram of the ultra micro-indentation (UMIS-2000) and acoustic emission systems.

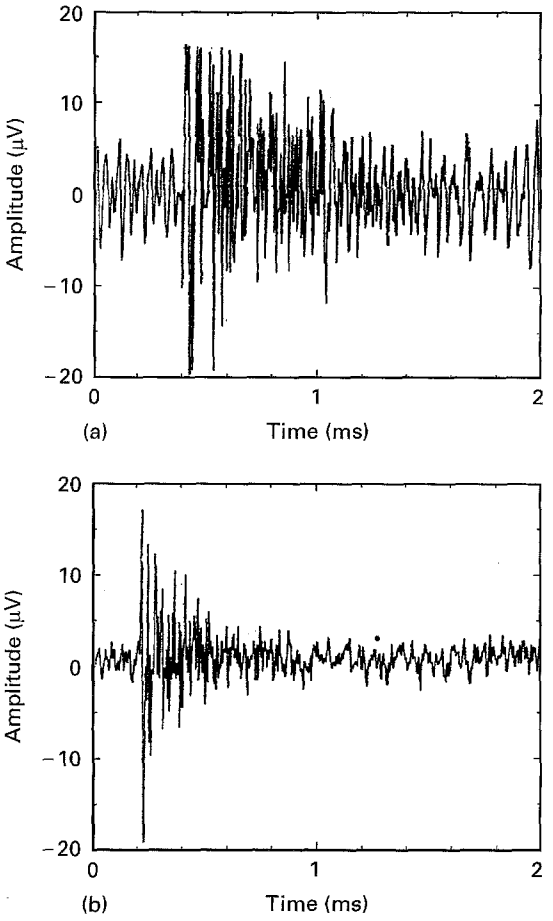

Figure 2 Typical waveform associated with acoustic emission from silicon during indentations recorded at (a) lower frequency (20–200 kHz), (b) higher frequency (100–300 kHz).

for optimization and quality assurance of such films. The present study attempted to provide more quantitative information and physical insight into the response of a brittle film on a softer substrate during indentation.

2. Experimental procedure

2.1. Samples

Two types of sample were used in this study. One was a single-crystal silicon 1.05 mm thick disc which was cut parallel to the [1 0 0] orientation. Thin films, 2.7 μm thick, were deposited on to single-crystal silicon wafers, using a filtered arc-vapour deposition system developed by Martin *et al.* [4]. Deposition took place at $\sim$ 623 K at a rate of 0.39 μm min^{-1} resulting in a fine columnar microstructure with a biaxial compressive stress of $\sim$ 1.4 GPa.

2.2. Micro-indentation

Indentation tests were carried out with an ultra micro-indentation system (UMIS-2000) developed by CSIRO [5]. This instrument has provision for testing and analysis with pointed- or spherical-tipped indentors. The nominal radius of the indentor used in this study was 5 μm, which agreed well with scanning electron micrographs of the indentor tip.

2.3. AE measurement

The acoustic emission sensor system in this study consisted of a high-sensitivity and low-noise integrated sensor, which had a resonant frequency of 300 kHz and the gain was 29 dB (M304, Fuji ceramics, Japan) [6]. The AE signals from the sensor system passed through a preamplifier which had a 40 dB gain and a 10 kHz to 1 MHz frequency response. The AE signal was further amplified, conditioned with various filter bandwidths and processed as ring-down counts (AECL 105, Acoustic Emission Consultants Ltd, UK), and the RMS voltage of the signals was measured with a voltmeter (931B, Fluke). The total gain of the AE system was 100 dB and the threshold level at the head amplifier was 1 μV. All data from the AE counter, and RMS voltmeter were recorded simultaneously with the force and displacement data by the PC controlling the UMIS-2000. Individual AE signals were recorded with a digital oscilloscope (PM3350, Philips). Fig. 1 shows a block diagram of measurement system. The AE sensor was mounted directly under the sample with cyanoacrylate glue.

3. Results

3.1. Force–displacement and AE signals from silicon

Typical AE waveforms of specific events during the indentation cycle of the silicon with different filters inserted in the AE signal path are shown in Fig. 2. Both levels of background noise and AE signals in the low frequency range (20–200 kHz), Fig. 2a, were higher than those in the high-frequency range (100–300 kHz), Fig. 2b. The duration of the AE signal for the low-frequency range was longer than that of the high-frequency range.

Figs 3 and 4 present typical data obtained on silicon for the force, accumulative sum of AE counts and RMS voltage of AE as a function of the displacement during indentation with the low-frequency range (Fig. 3) and the high-frequency range (Fig. 4), (a) loading, (b) unloading, respectively. The RMS voltage of the AE signals were different between the low- and high-frequency ranges. The low frequency range of these

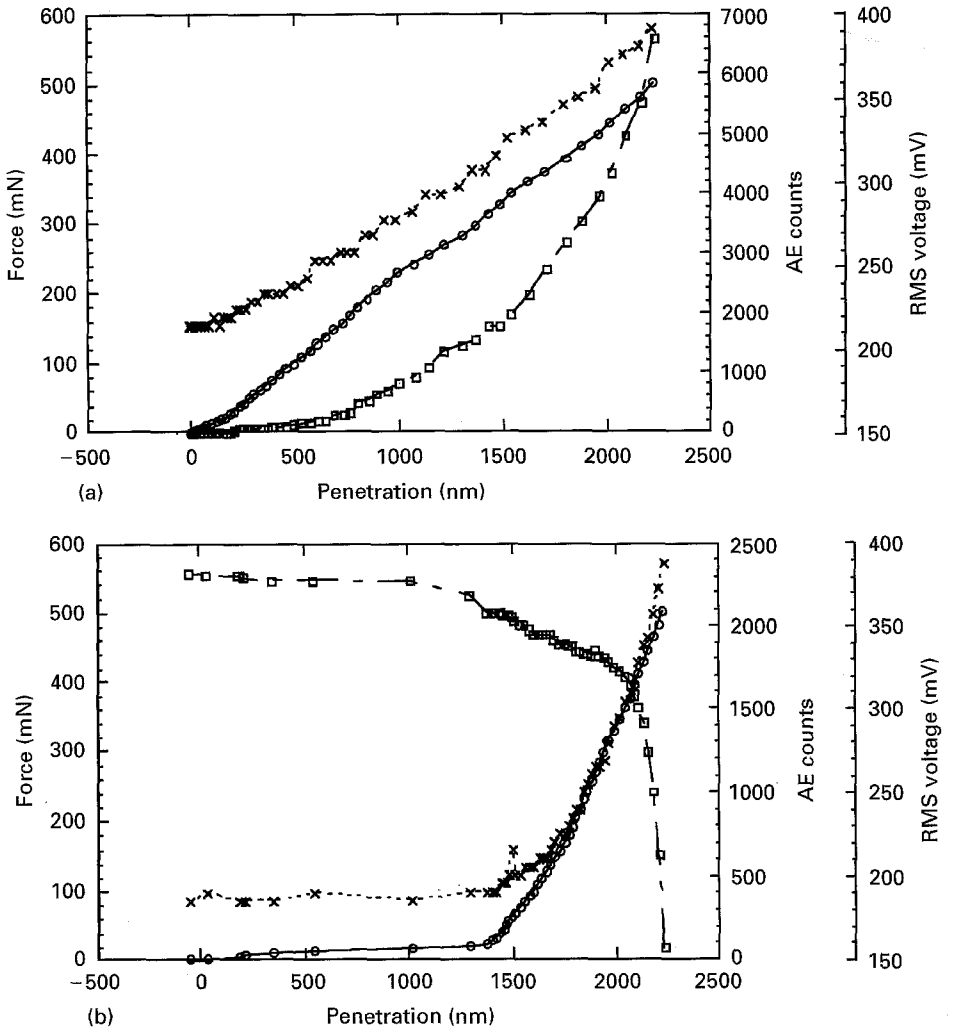

Figure 3 Force–displacement curve for the penetration of a 5 μm radius spherical indentor into silicon to a maximum force of 650 mN with a lower frequency band pass filter of AE: (a) loading data, (b) unloading data. (○) Force, (□) AE counts, (×) RMS voltage.

signals gradually increased with increasing force applied to the indentor. On the contrary, in the high-frequency band response, the background RMS voltage level was nearly the same level for both loading and unloading.

Analysis of the results in Fig. 4 shows five distinct stages of AE behaviour during the indentation of the sample. Stage I, typically from 0–100 mN was characterized by a steady linear increase in force and a slight increase in AE counts. From 100–320 mN, the number of AE counts rapidly increased indicating the onset of stage II. The stage II behaviour corresponded to slightly non-linear behaviour of the force–displacement curve and some large AE bursts of RMS voltage. At loads in excess of approximately 320 mN, transient non-linear behaviour of the force–displacement curve and many large AE bursts of RMS voltage were observed in stage III. The reduction of AE activity marks the onset of stage IV behaviour during unloading, which was characterized by a linear behaviour of the force–displacement curve and few AE counts. Finally, stage V, typically from 50–0 mN, corresponded with significant residual penetration and numerous AE events with small amplitude of AE bursts of RMS voltage.

3.2. Force–displacement and AE signals from TiN/Si

Typical AE waveforms of specific events for the 5 μm spherical indentor penetrating the 2.7 μm TiN film on silicon during indentation with different filters inserted in the AE signal path are shown in Fig. 5, (a) 20–200 kHz, (b) 100–300 kHz. In comparison with the data in Fig. 3, the duration of the events for the TiN film was shorter than that of the silicon.

Fig. 6 presents typical data for the penetration of the 5 μm indentor into the film on silicon during loading (Fig. 6a), and unloading (Fig. 6b) with the presence of the high-frequency filter. The data show three distinct stages of AE activity during the loading phase of indentation observed for indentation of silicon. Stage I, typically from 0–80 mN was characterized by a steady linear increase in force and very few AE counts. Stage II, from approximately 80–220 mN, showed some increase in AE counts at specific steps which corresponded to the onset of a non-continuous force–displacement curve. Above 220 mN, stage III, the number of AE counts increased continuously, which coincided with continuous deflection from the initial loading response. During unloading there also appears to be three distinct phases. Initially upon

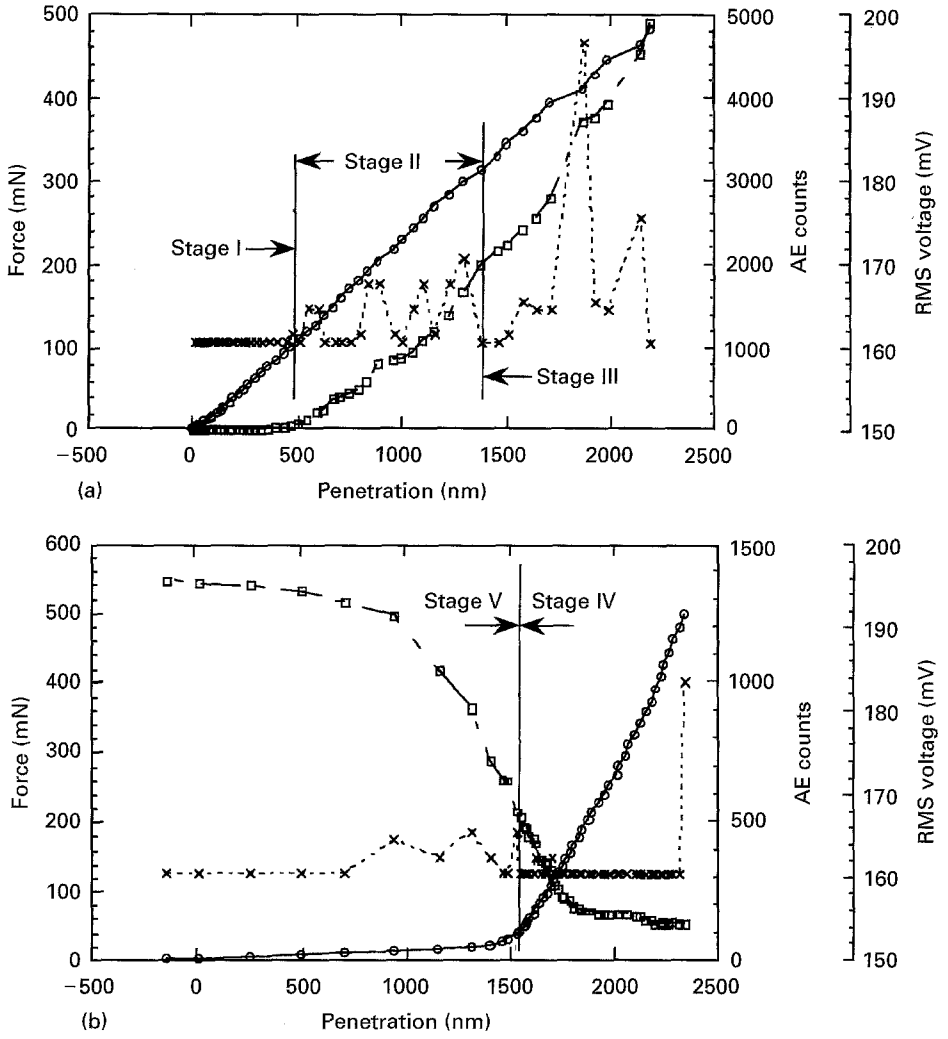

Figure 4 Force–displacement curve for the penetration of a 5 μm radius spherical indentor into silicon to a maximum force of 650 mN with a higher frequency band pass filter of AE: (a) loading data, (b) unloading data. (○) Force, (□) AE counts, (×) RMS voltage.

unloading, stage IV, there was a steady but limited number of AE counts. However at 120 mN, stage V, the response was characterized by a large burst of AE signal. Finally, stage V, typically from 100–0 mN, corresponded to few AE counts except upon final contact.

4. Discussion

4.1. Acoustic emission signals from indentation

The damage modes that developed during plastic indentation in brittle materials were investigated for different materials using spherical indentations by Evans and Wilshaw [7]. They determined the onset of cracking by recording acoustic emission sound and measured the detailed sequence of cracking formation and propagation events using high resolution optical microscopy during the indentation. Also acoustic emission signals from cracks in glass during indentation were evaluated by using the AE source characterization method of Kim and Sachse [8]. They reported that the AE signals from the lateral vent and penny-shaped cracks were similar to a typical Mode I crack, and the orientation of the penny-shaped cracks was determined from the AE source radiation pattern. Yasuda *et al.* [9] and Yoshida *et al.* [10] were able to evaluate fracture toughness of ceramics using the indentation method and acoustic emission. They detected the load for the onset of median cracking using acoustic emission signals during Vicker's indentation.

During indentation of silicon with a nano-indentation which we used, the RMS voltage indicated a different tendency between in the low-frequency range and the high-frequency response range (Figs 5 and 6). The RMS voltage of the low-frequency range also revealed a few bursts of signals of the order of a few tens of millivolts with increasing signal level. Therefore, the increasing RMS voltage in the low-frequency range may correspond to friction between the indentor and surface of the silicon. The high-frequency range may detect only transient deformation signals, such as transformation and cracking with the 300 kHz resonant sensor.

4.2. Fracture behaviour in silicon during indentation

The elastic stress field for plastic indentation was estimated by Evans and Wilshaw [7]. They found that

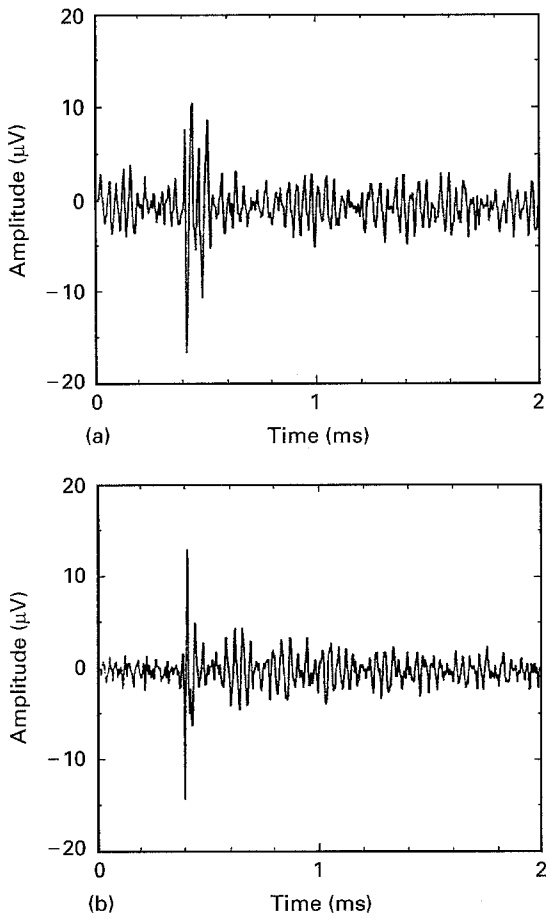

Figure 5 Typical waveform associated with acoustic emission from TiN film during indentations recorded at (a) lower frequency (20–200 kHz), (b) higher frequency (100–300 kHz).

the circumferential stress in the vicinity of the impression was tensile and the radial stress was much smaller than in the corresponding Hertzian field. This would explain the appearance of the radial cracks and the absence of any Hertzian cone cracks.

A typical scanning electron micrograph of the fracture patterns on the silicon surface loaded to 500 mN is shown in Fig. 7. This clearly indicates that radial and lateral cracks were forming, although there was some evidence that the lateral cracks may have initiated from a Hertzian cone crack, where a circular ring around the area of contact can be observed in parts, and a Hertzian cone crack is formed. Small radial cracks were observed at indentation loads under 350 mN.

During silicon indentation, the AE and force–displacement behaviour indicated five distinct stages, with three stages during loading and two-stages during unloading. Stage I was elastic region. In stage II of Fig. 4a, the first burst of AE signals was related to the volume dilation associated with the silicon II to silicon III phase transformation [2]. The phase transformation and similar phenomena were observed in stage V, during unloading in Fig. 4b, as "pop-out". At 400 mN in stage III, a Hertzian cone crack was formed with a large amplitude of AE burst. In stage IV, no discontinuity in the unload–deformation curve occurred. In stage V, after the transformation, some discontinuities occurred between the indentor and lifted surface of the silicon and some friction-related AE counts were observed.

4.3. Fracture process in silicon/TiN films

There are many possible explanations for the AE counts observed during the course of the present investigations, including microcracking, counts due to film cracking, substrate cracking, interface cracking, phase transformation of silicon, and contact slippage between indentor and substrate, to name just a few. The aim here is to attempt to correlate the observed AE counts with specific features of the force–displacement curves and SEM observations of normal and cross-sectional views of the contact damage.

The initial loading, stage I, is undoubtedly elastic, which enables an estimate of the mean contact pressure at the critical load for the onset of the first AE counts. From Field and Swain [11], a simple estimate of contact pressure is given by

$$P_m = P_c/\pi\delta R \quad (1)$$

where P_c is the critical load, δ is the displacement and R is the indentor radius. In the present observations the values of P_c and δ were 140 mN and 320 nm, respectively, that is $P_m = 28$ GPa. The actual tensile stresses within the film about the contact site were more difficult to estimate, although Djabella and Arnell [12], using finite element analysis, indicated that the stresses were very dependent upon the ration of the E moduli for film and substrate.

At heavier loads beyond P_c, stage II, further minor steps in the force–displacement record occurred which coincided with distinct AE counts and sharp increases in RMS voltage output. The isolated nature and coincidence of all these events suggests that continued isolated film cracking occurs. At heavier loads entering stage III, the AE activity, RMS voltage and continued deflection suggest near continuous cracking about the contact site.

SEM observations of the contact site after heavier loads (650 mN), Fig. 8, suggests the contact appears to have been "plastic" with the development of radial cracks emanating from the contact circle. Other SEM observations at lower indentor loads reveal that the onset of radial cracking took place at ~200 mN, this was almost identical to the onset of stage III behaviour mentioned above.

During unloading, stage IV, the initial response was almost entirely elastic with a few minor AE counts of relatively low intensity. This would suggest the possible onset of interfacial delamination. Upon further unloading, Stage V, intense AE activity and an increase in RMS voltage occur, which coincide with a discontinuity in the unloading slope as "pop-out" associated with the silicon II to silicon III phase transformation. Further AE counts and low RMS intensity of such activity during continued unloading, stage VI, indicates that lateral cracking may be occurring. Cross-sectional SEM observation of the indentation impressions at intermediate (350 mN) and heavier loads (650 mN) provided strong support for the above interpretation. The lower load impression, Fig. 9,

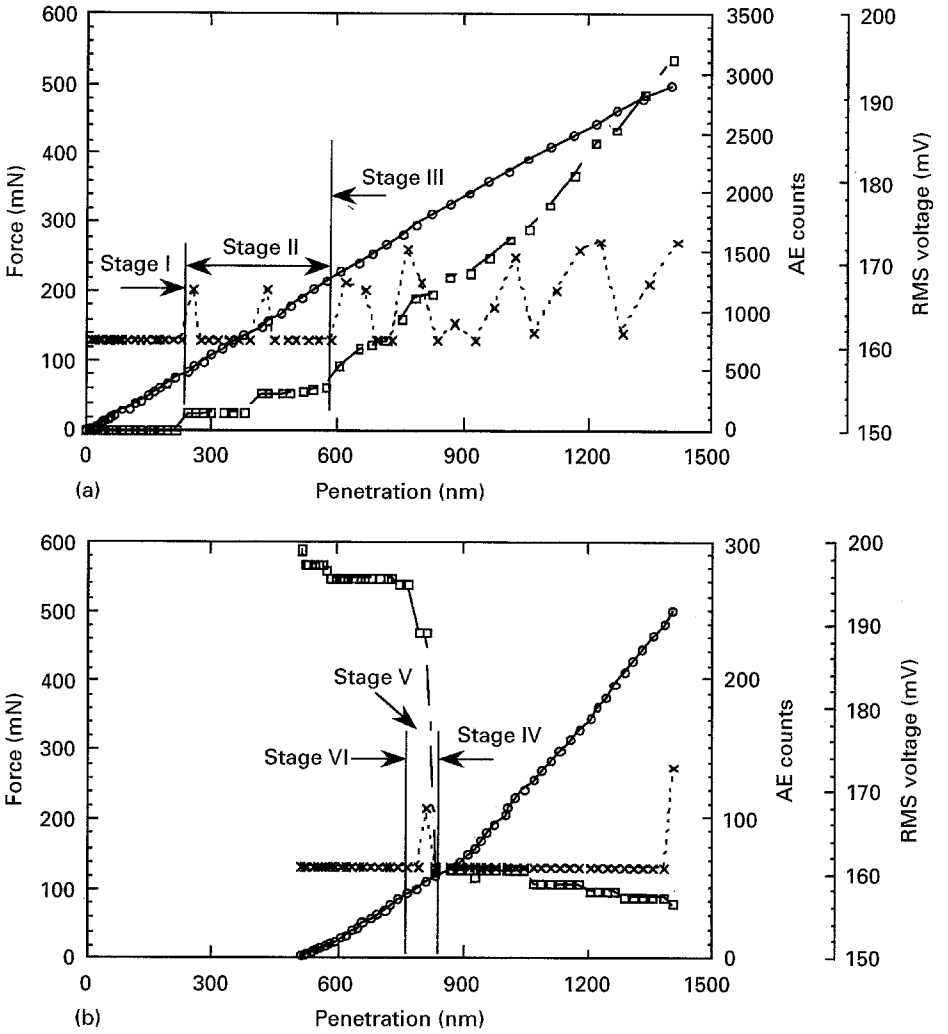

Figure 6 Force–displacement curve for the penetration of a 5 μm radius spherical indentor into the TiN film on silicon to a maximum force of 650 mN with a higher frequency band pass filter of AE: (a) loading data, (b) unloading data. (○) Force, (□) AE counts, (×) RMS voltage.

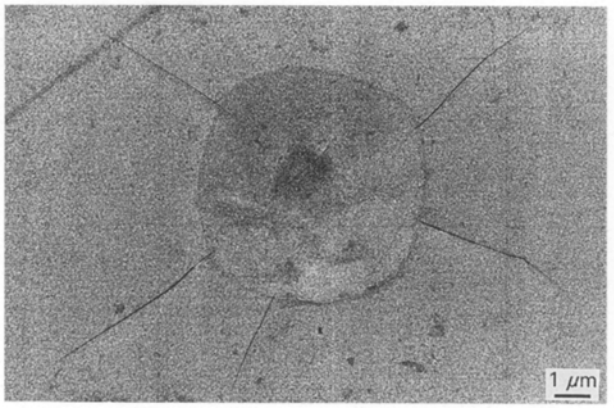

Figure 7 Scanning electron micrograph of the residual impression in the silicon upon indenting with a 5 μm radius indentor to a maximum force of 500 mN.

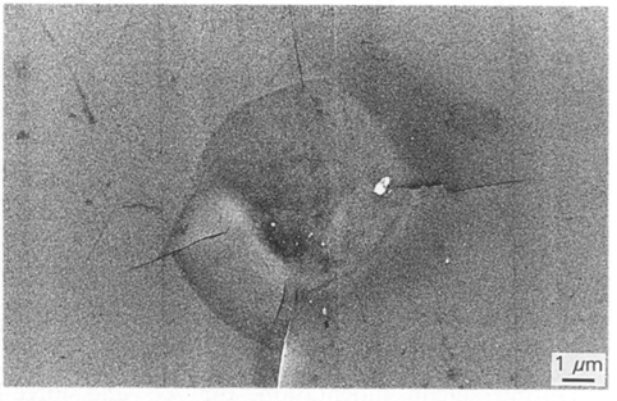

Figure 8 Scanning electron micrograph of the residual impression in the TiN film upon indenting with a 5 μm radius indentor to a maximum force of 500 mN.

shows clear evidence of the highly columnar structure of TiN film that had undergone two shear fault cracks along the columnar grain boundaries. There was evidence for some "plastic"-like deformation directly beneath the contact site, as well as an interfacial delamination crack outside the contact area. On the left-hand side of the micrograph, the crack has initially propagated into the substrate before extending along the interface. At higher loads, 650 mN, Fig. 10, much more extensive evidence for shear faulting of the TiN film took place as well as subsurface "plastic" deformation. Fig. 10, which was a cross-section of Fig. 8, indicates that the apparent plastic deformation of the residual impression was accommodated by shear faulting and "plastic" deformation of the silicon substrate. It was also clearly

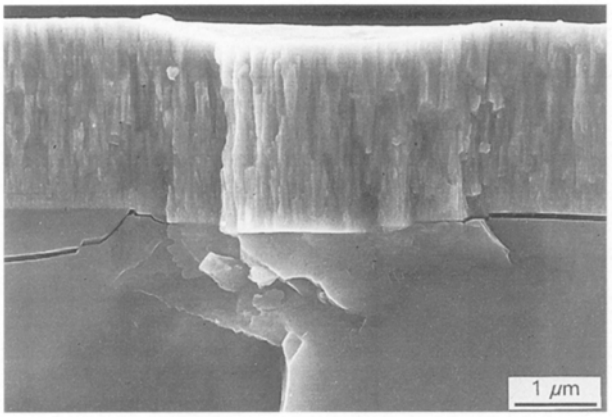

Figure 9 Scanning electron micrograph of a cross-section through an indentation made with a force of 650 mN on to 2.7 μm thick TiN film on silicon.

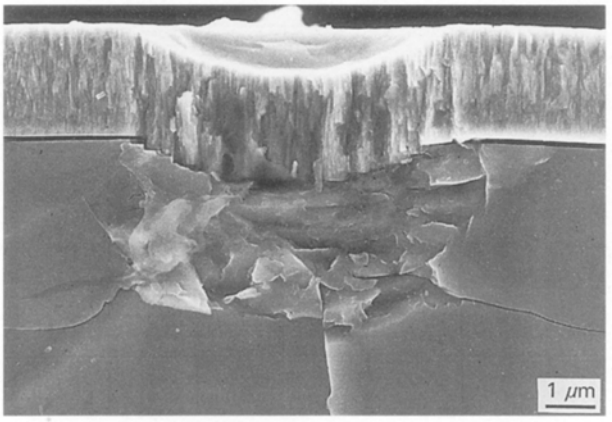

Figure 10 Scanning electron micrograph of a cross-section through an indentation made with a force of 350 mN on to 2.7 μm thick TiN film on silicon.

evident that interfacial delamination cracks were present.

The present SEM observations, force–displacement and AE data, provide clear indication of the indentation behaviour of the TiN film on silicon during loading and unloading with a 5 μm radius indentor. Stage I coincides with the elastic response of the system and estimated critical contact pressure was well in excess of that required to induce "plastic" deformation of the silicon substrate. Stage II marked the development of film cracking with a circular crack about the diameter of contact that propagates through the film in a shear faulting manner. Stage III coincided with the formation of radial cracks within the film emanating from the contact diameter, as well as further circular cracks within the film and extensive "plastic" deformation of the substrate. During unloading, the initial response, stage IV, was almost entirely elastic with some evidence for interfacial delamination. At a critical unload, stage V, which appeared to be when the silicon underwent a volume-expanding reverse phase transformation, major AE counts associated with film cracking (perhaps continued radial cracking), as well as delamination occur. Continued unloading, stage VI, resulted in low-intensity AE activity, suggestive of continued interfacial delamination.

5. Conclusion

The present measurements of AE activity, force–displacement response and SEM observation have provided an excellent insight into the physical behaviour of brittle films on less hard brittle substrates during indentation.

In the case of silicon single crystals, the AE data strongly support the observations previously made by Weppelmann *et al.* [2], in that the onset of deformation was associated with a phase change, and the "pop-out" event during unloading was also related to a reverse phase transformation. The latter event was associated with little AE activity and most of the major AE events during the loading and unloading stages were related to cracking.

The AE activity suggested that the heavier load data for a spherical indentor penetrating a TiN film on silicon can be considered as six stages. The results suggest virtually no plastic deformation of the brittle film occurs, but rather shear faulting of the film and "plastic" deformation of the substrate. These present observations have clear implications for interpretation of force–displacement data generated with pointed indentations on brittle substrates.

Acknowledgements

The authors thank Dr Phil Martin and Avi Bendavid for the TiN film deposition.

References

1. E. R. WEPPELMANN, X-Z. HU and M. V. SWAIN, *Int. J. Adhes. Sci. Techol* **8** (1994) 611
2. E. R. WEPPELMANN, J. S. FIELD and M. V. SWAIN, *J Mater. Res.* **8** (1993) 830.
3. T. P. WEIHS, C. W. LAWRENCE, B. DERBY, C. B. SCRUBY and J. B. PETHICA, *Proc. MRS Symp.* **239** (1992) 361.
4. P. J. MARTIN, R. P. NETTERFIELD and T. J. KINDER, *Thin Solid Films* **193/194** (1990) 77.
5. T. J. BELL, A. BENDELI, J. S. FIELD, M. V. SWAIN and E. G. THWAITE, *Metrologia* 28(1991/1992) 463.
6. M. SHIWA, H. INABA, S. H. CARPENTER and T. KISHI, *Mater. Eval.* **50** (1992) 868.
7. A. G. EVANS and T. R. WILSHAW, *Acta Metall.* **24** (1976) 939.
8. K. Y. KIM and W. SACHSE, "Progress in Acoustic Emission II" (JSNDI, Japan, 1984) 163.
9. E. YASUDA, Y. TANABE, K. MIYAHARA, T. FUKAI, S. KIMURA and H. HATANO, *Jpn. J. Ceram.* **95** (1987) 503.
10. K. YOSHIDA, H. GOHDA, H. TAKAGI and K. SASAKI, *Jpn. J. NDE* **40** (1992) 725.
11. J. S. FIELD and M. V. SWAIN, *J. Mater. Res.* **8** (1993) 137.
12. H. DJABELLA and R. D. ARNELL, *Thin Solid Films* **213** (1992) 205.

Received 3 January
and accepted 18 March 1996